scientific reports

Check for updates

OPEN

Joint simulation and experimental verification of electromechanical-hydraulic of hydraulic excavator working device

Mei Xin[1], Zhigui Ren[1,2]✉, Yiding Yu[1], Yudong Tian[1], Heng Zhang[1], Kaitao Ren[1] & Yijian Zhang[1]

To rigorously evaluate the electromechanical-hydraulic coupling performance of a hydraulic excavator's working device under authentic operating loads, this study presents a field-data-driven co-simulation framework applied to a 20-ton backhoe hydraulic excavator. Full-scale digging experiments were conducted at the Liuzhou test site, where boom, arm, and bucket cylinder pressures, together with joint angles, were synchronously sampled to back-calculate the real-time excavation resistance. This measured resistance was then imported as an external load into a three-dimensional dynamic model established in ADAMS and bidirectionally coupled with the electro-hydraulic system model developed in AMESim. For three representative digging depths: surface digging, 1 M digging, and 2 M digging, the maximum discrepancy between simulated and measured cylinder pressures was 6 MPa (about 15%), while the correlation coefficients of the pressure traces ranged from 0.907 to 0.975, showing excellent agreement. The observed deviations are primarily attributed to load uncertainty; nevertheless, the proposed model accurately captures the dynamic interaction between the electro-hydraulic system and the mechanical system, offering a reliable experimental foundation for performance assessment and digital-twin applications of hydraulic excavator working device.

Keywords Hydraulic excavator, Working device, Joint simulation, Experiment verification

Hydraulic excavators are pivotal equipment in engineering construction, and the performance of their working mechanisms directly impacts operational efficiency[1]. With the diversification of user demands and the development of digital twin technology, how to shorten the design and development cycle of hydraulic excavators has become a core aspect of corporate competitiveness and a hot research topic among many scholars. In recent years, numerous scholars have focused on utilizing various software tools to calculate, simulate, and model the operational characteristics of excavator working mechanisms, significantly improving design quality and reducing design time before prototype manufacturing.

Mechanical and hydraulic characteristics are the most important indicators of working device performance. In terms of mechanical characteristics, Zhang et al.[2] conducted dynamic simulations of excavator working devices using virtual prototype technology, quantifying the transient load peaks of hydraulic cylinders and hinge points. They provided an integrated modeling, verification, and optimization approach with low time and cost, offering insights for the design of actual performance parameters. Jiang et al.[3] used an empirical load model in ADAMS software to output the transient peak load spectra of the excavator's working device hinge points and hydraulic cylinders, verifying the reliability of the parametric virtual prototype process in predicting excavator dynamics. In terms of hydraulic characteristics, Zhu et al.[4] designed an automatic leveling system for a three-degree-of-freedom hydraulic robotic arm. Through AMESim-PID electro-hydraulic closed-loop simulation, they validated the feasibility of the boom drive control system design and proposed positioning and leveling operation workflows suitable for engineering applications, which were verified to meet the requirements of high construction efficiency and low cost. Bao et al.[5] established an electromechanical-hydraulic joint simulation model in the AMESim software and validated the bucket trajectory, pump flow/pressure, and load matching issues through full-cycle simulation, providing a reliable control strategy and parameter calibration framework for joint simulation. Currently, single-software simulation is relatively mature and produces accurate results.

[1]College of Mechanical Engineering, Shaanxi University of Technology, Hanzhong 723001, Shaanxi, China. [2]Key Laboratory of Industrial Automation, Shaanxi University of Technology, Hanzhong 723001, Shaanxi, China. ✉email: zguiren2014@163.com

However, the excavator's working device is a highly coupled electromechanical-hydraulic system, and the coupling effects between systems are difficult to obtain through individual simulations.

With the cross-development of multibody dynamics and fluid transmission theory, recent research has begun employing integrated simulation models. Through real-time data interaction, these models reveal system-level dynamic characteristics. Multidisciplinary collaborative simulation and optimization design have further enhanced critical equipment performance, establishing a new paradigm for analyzing complex operating conditions[6–8]. Park et al.[9] Established a dynamic system and hydraulic model for real-time simulation of large excavators, and divided the entire model into multiple sub-models to ensure the real-time performance and accuracy of the simulation. Under the framework of hydraulic drive systems, Jasiwal et al.[10] proposed a state estimator that combines a multibody model with indirect Kalman filtering. This state estimator accurately estimates the working cycle and hydraulic pressure of the coupled multibody system. Both Jasiwal et al.[11] and Rahikainen et al.[12] employed semi-recursive formulas in the simulation of hydraulic-driven multibody systems, demonstrating that the proposed method has great potential in efficiently simulating the combination of multibody dynamics systems and hydraulic systems.

Zhou et al.[13] utilized ADAMS and AMESim to construct an electromechanical-hydraulic joint simulation model of an excavator's working mechanism, conducting an in-depth study on motion trajectory control under typical digging conditions. They successfully achieved closed-loop control of the motion trajectory; however, their research on data interaction and sharing between the hydraulic system and mechanical system remains insufficient, and it does not address the dynamic characteristics analysis of multiparameter coupling under complex operating conditions. Zhang et al.[14] established a joint simulation model in AMESim and Simulink, verifying a trajectory error accuracy of less than 20 mm under straight-line digging conditions. However, this study was limited to single-level digging, and the joint simulation model was not established in higher-precision dynamics software. Wang et al.[15] developed an automatic control system for excavators by modifying, modeling, and designing control programs for multiple subsystems. However, due to limitations in the hydraulic system, the control process exhibits some delay. Gan et al.[16] and Liu et al.[17] developed a multisystem joint simulation model for hydraulic excavator systems based on the Functional Model Interface (FMI), revealing the significant influence of load on the excavator's dynamic behavior and the force characteristics of each working stage. However, experimental validation of the simulation model remains insufficient.

In conclusion, the achievements of previous studies have provided advanced disciplinary backgrounds and reference ideas for this research in aspects such as multidisciplinary collaborative design optimization, modular modeling and parallel solution strategies, multisystem state estimation methods, and the stability and real-time performance of joint simulation. The implementation of these works all relies on a simulation platform that can accurately reflect the coupling of multiple systems. Therefore, the construction of an experimentally verified and highly reliable electromechanical-hydraulic joint simulation model is the key cornerstone towards the above advanced applications.

Against this background, this study takes the working device of the hydraulic excavator as the research object for exploration. Although many scholars have been dedicated to the joint simulation of mechanical and hydraulic performance in recent years, due to the inaccuracy of parameters such as hydraulic valves and the lack of actual resistance data for mining, the accuracy of the model has declined and it cannot be effectively verified. To address this issue, the research team collaborated with enterprises to enhance the accuracy of valve group parameter Settings. They established a joint simulation model using AMESim and ADAMS, and based on the mining resistance test calculation method, verified the joint simulation model with measured data.

Establish an electromechanical-hydraulic joint simulation model for the excavator working device

Establish a dynamic simulation model of the working device

Taking a 20-ton backhoe hydraulic excavator as the research subject, a 3D model was created in SolidWorks based on the structural parameters of the actual excavator's working equipment. In the model, manufacturing holes, chamfers, welds, and other features with minimal overall impact on dynamics were appropriately simplified without compromising the main performance of the working equipment. The boom, arm, and bucket of the working device were defined with Q345 material, whose performance parameters are shown in Table 1. As listed in Table 2, constraint types were applied to each component after the model was imported into ADAMS[18]. These included translational, revolute, co-linear constraints, and others, adhering to the actual kinematic relationships of the mechanism. This ensured the model's degrees of freedom matched those of the real system.

After adding the constraints, use the corresponding ADAMS/View tool to verify the model. As shown in Fig. 1, the result is that there are no overconstrained equations, and the model verification is correct.

Combined simulation model of mechanical and electro-hydraulic systems

Establishment of an electro-hydraulic system model

The electro-hydraulic control system of the hydraulic excavator's working device consists of an electronic control module, a hydraulic drive unit, and mechanical actuators. Its core function is to control the operation

Material	Elastic modulus/GPa	Density/(kg m^3)	Poisson's ratio
Q345	206	7850	0.3

Table 1. Material performance parameters.

Part1	Part2	Constraint name
Base	Base	Fixed
Base	Boom hydraulic cylinder	Revolute
Base	Boom	Revolute
Boom hydraulic cylinder	Boom hydraulic cylinder piston rod	Translational
Boom hydraulic cylinder piston rod	Boom	Co-linear constraints
Arm hydraulic cylinder	Boom	Revolute
Arm hydraulic cylinder	Arm hydraulic cylinder piston rod	Translational
Boom	Arm	Revolute
Arm hydraulic cylinder piston rod	Arm	Co-linear constraints
Arm	Bucket hydraulic cylinder	Revolute
Bucket hydraulic cylinder	Bucket hydraulic cylinder piston rod	Translational
Rocker rod	Arm	Revolute
Rocker rod	Connecting rod	Spheric pair
Bucket hydraulic cylinder piston rod	Connecting rod	Co-linear constraints
Bucket	Arm	Cylindric pair
Connecting rod	Bucket	Revolute

Table 2. Constraint type between parts.

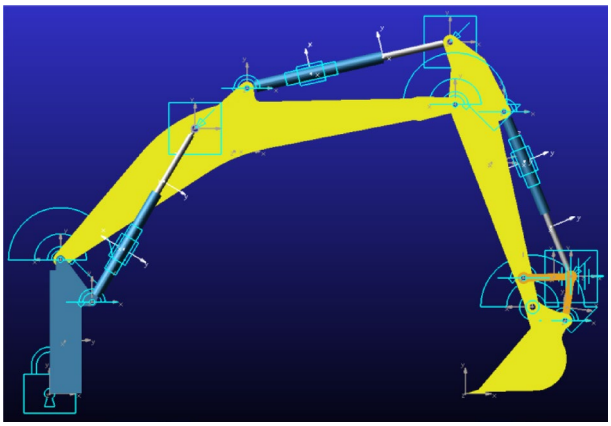

Fig. 1. Model diagram of the excavator working device.

Hydraulic cylinder parameters	Piston diameter/mm	Rod diameter/mm	Length of stroke/mm
Boom hydraulic cylinder	120	85	1300
Arm hydraulic cylinder	135	95	1490
Bucket hydraulic cylinder	115	80	1120

Table 3. Structural parameters of hydraulic cylinders.

of hydraulic valves via electrical signals, thereby regulating the flow and pressure of hydraulic cylinders to drive the working device to perform predetermined actions[19]. A distributed collaborative solution method is used to achieve coupled modeling of the electromechanical-hydraulic system, with the specific construction process as follows:

Select standard components from the AMESim standard component library, establish a model based on the hydraulic system principles of the excavator's working device, and, given the simplification of the model in simulation, select a fixed-displacement pump to provide the pressure oil source, with a three-position four-way hydraulic servo valve driving the double-acting hydraulic cylinder. The stroke parameters of the servo valve spool must meet the desired displacement input in the control components. The structural parameters of the hydraulic cylinder are consistent with those in the ADAMS dynamics model, as shown in Table 3. The viscous friction coefficient is a key parameter affecting the dynamic accuracy and energy efficiency of the hydraulic cylinder. During the simulation process, the parameters are adjusted to maintain high accuracy while minimizing energy efficiency loss.

Establish a combined electromechanical-hydraulic simulation model

Interface configuration is the most critical aspect of joint simulation, as the interface serves as the pathway for data exchange between two software systems. The hydraulic excavator's working device comprises three circuits with identical principles. Figure 2 illustrates the electromechanical-hydraulic joint simulation schematic for one of these circuits. The diagram illustrates data exchange between the mechanical and hydraulic systems via an interface for force and displacement. The mechanical system's FMU contains all information from the working device's dynamic model. Component 7 (force sensor) receives hydraulic pressure transmitted from the hydraulic system and relays the signal to the mechanical system, driving the working device to perform excavation. The mechanical system continuously transmits cylinder displacement data to component 8 (displacement sensor) in the hydraulic system, completing the closed-loop transfer of force and displacement.

In the ADAMS/Controls module, define the input and output variables of the mechanical system:

Input process: The AMESim hydraulic system inputs the forces acting on the three hydraulic cylinders into the ADAMS mechanical system;

Output process: The ADAMS mechanical system inputs the displacement of the three hydraulic cylinders into the AMESim hydraulic system.

Using the Functional Model Interface (FMI) in ADAMS/Controls, the dynamic model is exported as a corresponding Functional Model Unit (FMU) for AMESim to call, enabling joint simulation. Connect it to the hydraulic system model via sensors, set the unit conversion parameters and simulation time, and start the simulation.

Principles of joint simulation model verification and experimental testing process

Principles of joint simulation model verification

The working mechanism of a hydraulic excavator has multisystem coupling characteristics, which can easily lead to cumulative errors. To verify the correctness of its simulation model, it is necessary to verify the accuracy of kinematics, dynamics, and the joint simulation layer by layer.

Kinematic simulation verification is to test the geometric motion relationship, that is, whether the trajectory of the actuator during motion conforms to the experimental values. This study verifies the envelope diagram of the excavator's working device. Dynamics simulation verifies the dynamic response of the working device under force. This study verifies the force conditions at the hinge points of the working device under load conditions. Joint simulation and validation involves driving the movement of working devices within a mechanical system through hydraulic cylinder pressure, thereby comparing experimental hydraulic cylinder pressure values with simulated values. Figure 3 illustrates the complete process of joint simulation and validation, showing how cylinder pressure and cylinder displacement are transmitted via FMU. The correctness of the joint simulation model is verified by comparing the simulation results of the cylinder pressure in the joint simulation with the experimental results.

Experimental testing process

This study used a 20-ton backhoe hydraulic excavator as the test object and conducted tests on three levels of soil conditions at a certain test site. The experiment used a multichannel data acquisition system to simultaneously record various sensor data. Figure 4 is a field test diagram.

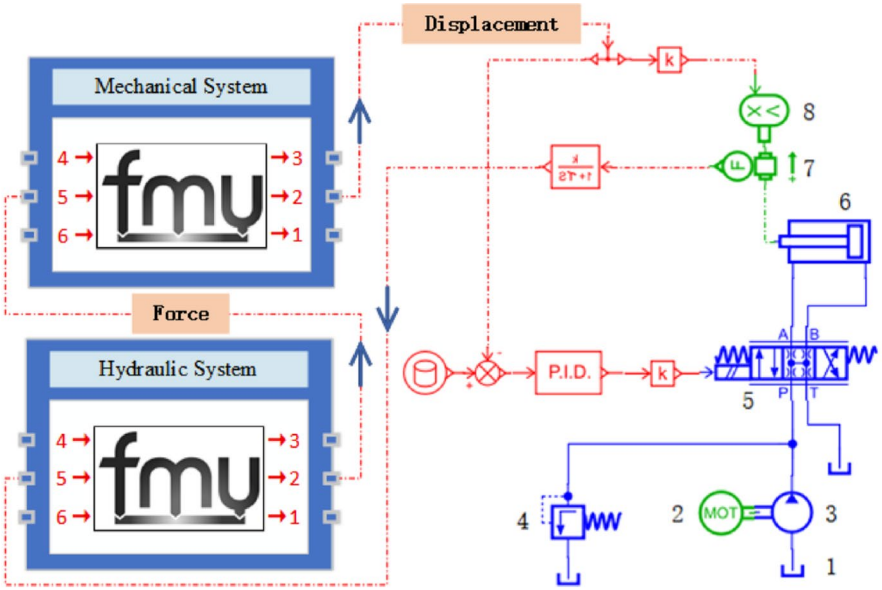

Fig. 2. Schematic diagram of the joint simulation model of the working device of a hydraulic excavator.

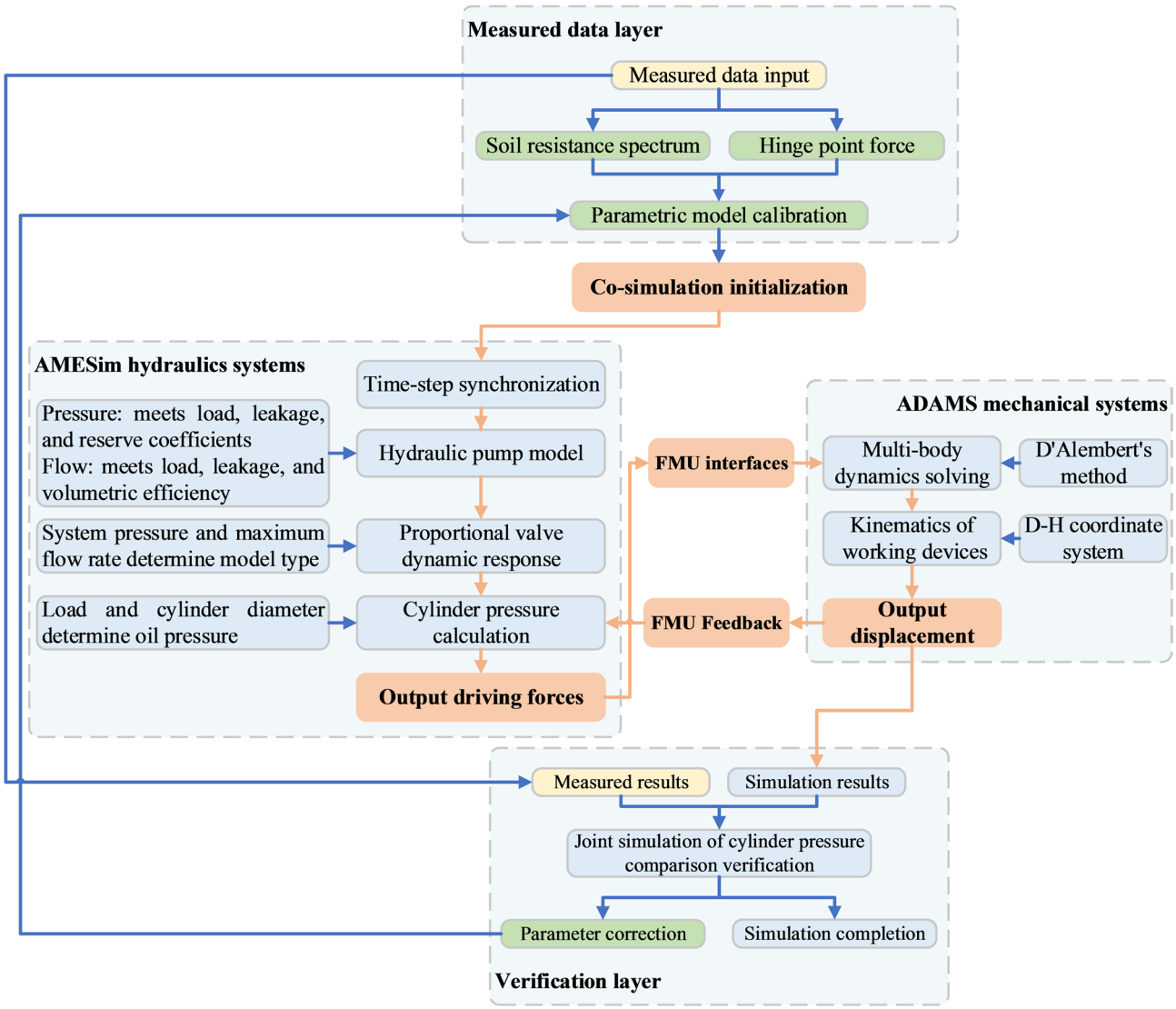

Fig. 3. Joint simulation and verification flowchart.

Fig. 4. On-site test diagrams of excavators at different digging depths.

The testing content comprises three parts:

(1) Angular displacement test: By installing angular displacement sensors at key hinge points of the working device, the sensor's rotational axis remains concentrically fixed to the working device's pin shaft via a coupling. This enables real-time monitoring of three sets of rotation angles, used to reconstruct the spatial orientation and motion trajectory of the working device. The three hinge points are: the hinge point between the base and the boom, the hinge point between the boom and the dipper arm, and the hinge point between the dipper arm and the bucket. These correspond to points A, B, and G in Fig. 5. The three sets of rotation

angles are: the rotation angle of the boom relative to the base, the rotation angle of the arm relative to the boom, and the rotation angle of the bucket relative to the arm.

(2) Hydraulic pressure test: Pressure sensors are installed in both the rod and non-rod chambers of the boom cylinder, arm cylinder, and bucket cylinder. These sensors record the dynamic pressure changes within each hydraulic cylinder during excavation operations. The installation locations correspond to the pre-designated pressure test points on the rod and non-rod chambers of each hydraulic cylinder.

(3) Stress Testing: Utilizes strain gauges to measure strain at critical locations, deriving stress distribution through resistance changes. This method verifies the structural strength of working equipment and the accuracy of excavation resistance models. Measurement points on the boom include: the inner and outer sides at the lower root connecting to the chassis, the pivot ear plate connecting to the boom hydraulic cylinder, the pivot ear plate connecting to the arm stick hydraulic cylinder, the pivot ear plate connecting to the arm, and the upper and lower cover plates at the boom midpoint. Arm measurement points include: the hinge ear plate connecting to the boom, the hinge ear plate connecting to the bucket hydraulic cylinder, the upper and lower cover plates at the mid-section of the arm, the hinge ear plate connecting to the arm hydraulic cylinder, the hinge ear plate connecting to the bucket, and the hinge ear plate connecting to the rocker arm. Bucket measurement points include: the hinge ear plate connecting to the arm, the hinge ear plate connecting to the connecting rod, the back of the cutting edge, and the area near the bucket tooth mount.

This test conducted multiple experiments on three typical digging depths of hydraulic excavators, testing the relative angles of the working devices at three digging depths and the pressure changes of three sets of hydraulic cylinders over time. The three different digging depths selected were surface digging, 1 M digging, and 2 M digging. Surface digging is commonly used in land leveling and site clearance operations, 1 M digging is commonly used in infrastructure construction, such as ditch excavation and pipeline laying, and 2 M digging is commonly used in subway construction and deep mining. The selection of these three digging depths can basically cover the performance of hydraulic excavators at different digging depths and in different operating environments, thereby providing a deeper understanding of the performance characteristics, stress conditions, and optimization space of their working devices.

By collecting hydraulic cylinder pressure data at different digging depths and rotational displacement parameters of various components, the active-side calculation method for normal incomplete digging resistance developed by the author's team can determine the digging resistance[20]. This model accounts for the following constraints: Stability: The excavator does not tilt forward or backward during digging; Adhesion: The excavator does not move relative to the ground; Maximum locking force of the locking cylinder: Ensures no stretching or compression occurs when all cylinders are locked; During bucket digging: When substituting the maximum working thrust of the bucket cylinder as the hydraulic cylinder thrust in calculations, the resultant moment of the force system acting on the bucket at the arm-bucket hinge point is less than or equal to zero; During arm digging: When the maximum working thrust of the arm cylinder is substituted as the cylinder thrust in calculations, the resultant moment of the force system acting on the arm at the boom-arm linkage point must

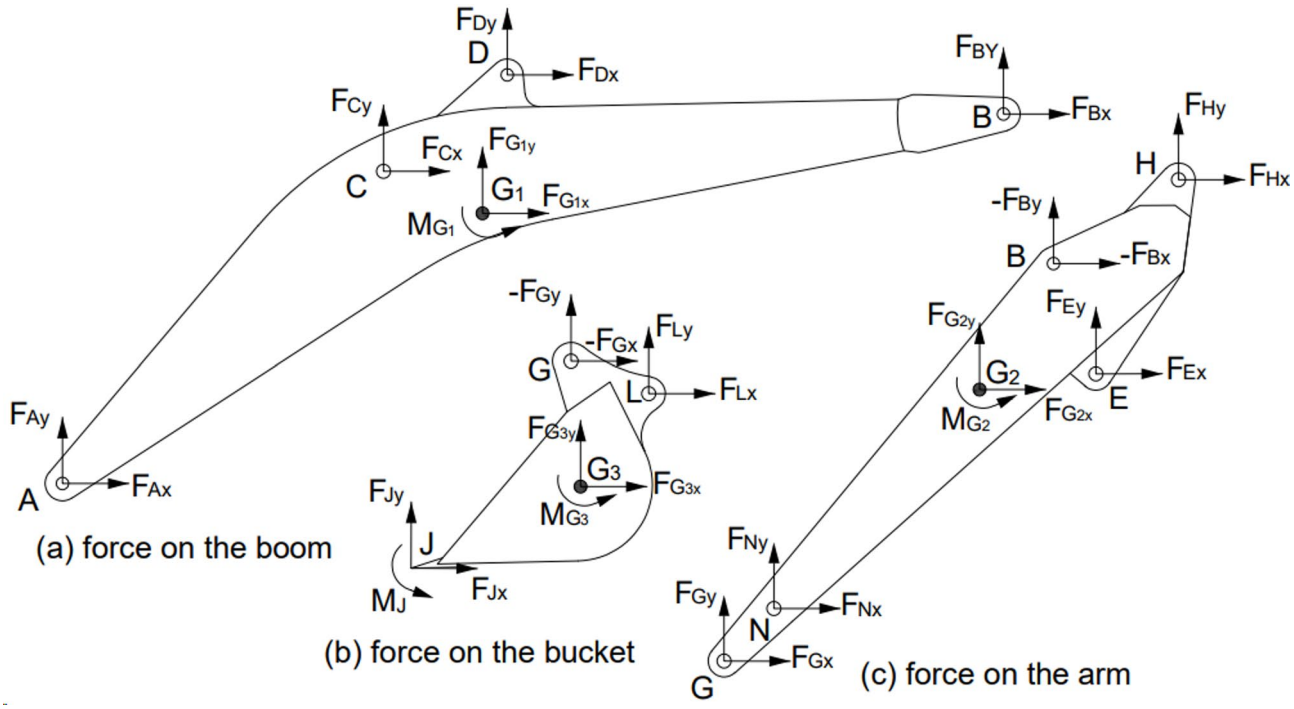

Fig. 5. Force diagram of each component in the global coordinate system.

Mobile subdrive	Function expression
Boom hydraulic cylinder and boom hydraulic cylinder piston rod	step(time,0,0,2,405) + step(time,8,0,10,-1181)+ step(time,16,0,18,1181)
Arm hydraulic cylinder and arm hydraulic cylinder piston rod	step(time,0,0,2,-731) + step(time,4,0,6,1490)+ step(time,12,0,14,-1490)
Bucket hydraulic cylinder and bucket hydraulic cylinder piston rod	step(time,0,0,2,-712) + step(time,2,0,4,1120)+ step(time,6,0,8,-548) + step(time,10,0,12,-373)+ step(time,14,0,16,-175)

Table 4. Driver function expressions.

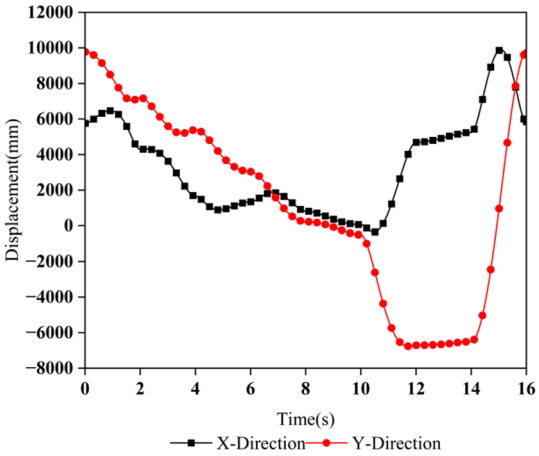

Fig. 6. Bucket tooth tip trajectory.

be less than or equal to zero. Subsequently, the forces at each component's hinge points are determined through force analysis using the d'Alembert's static method.

From the above analysis, it can be seen that by collecting the hydraulic cylinder oil pressure and the motion parameters of each component relative to the coordinate system of the previous component, the forces acting on each hinge point of the working device can be calculated. These values can then be compared with the hinge point force values obtained from simulation to verify the correctness of the model from a mechanical characteristics perspective. Additionally, by comparing the oil pressure experimental values with the simulation values, the correctness of the joint simulation model can be verified from a hydraulic characteristics perspective.

Simulation and verification results analysis

Kinematics simulation and verification

Kinematics simulation is an important method for verifying the motion characteristics of mechanical systems through preset driving conditions. The reliability of the model is evaluated by analyzing the degree of conformity between the actual motion trajectory of the end effector and the theoretical design trajectory. For hydraulic excavators, the drawing of the working envelope diagram is a key step in kinematic analysis. This diagram not only intuitively displays the effective working range of the equipment but also effectively identifies potential interference phenomena that may occur among moving components during operation[21].

In this study, the step function is used as the driving signal in the hydraulic cylinder motion control, and the specific implementation method is to set the STEP function on the moving pair of each hydraulic cylinder. Table 4 lists in detail the mathematical expressions of the driving functions of the three actuators of the boom hydraulic cylinder, arm hydraulic cylinder, and bucket hydraulic cylinder, and their parameter settings. This drive mode can better simulate the step response characteristics of the hydraulic system under actual working conditions.

In the post-processing module, the coordinates of the bucket tooth tip points plotted in the x and y directions are shown in Fig. 6, and the excavator envelope diagram is shown in Fig. 7. The key parameters of the simulation results were compared with the calculation results, as shown in Table 5. Among them, the relative error of the maximum unloading height is 4.53%, and the relative error of the maximum digging height is only 1.21%. All errors are within the allowable range, verifying that the simulation model has high accuracy.

Dynamic simulation and verification

The correctness of the model is verified by analyzing the mechanical response of each component under external loads and comparing the force conditions at key hinge points under specific digging resistance. The method for determining external loads under composite digging conditions is as follows: the digging resistance generated by the bucket contacting the material can be decomposed into three components: tangential resistance along the

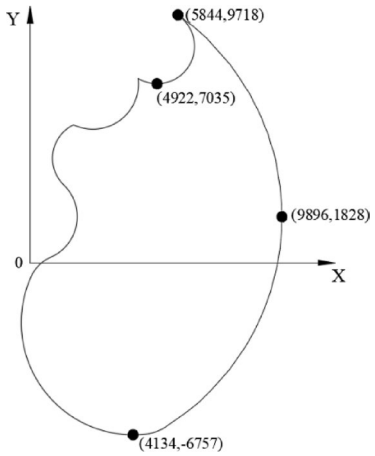

Fig. 7. Excavator envelope diagram.

Data comparison	Maximum digging radius/mm	Maximum unloading height/mm	Maximum digging height/mm	Maximum digging depth/mm
Calculated value	10,280	6730	9600	6600
Simulation value	9896	7035	9718	6757
Error	3.74%	4.53%	1.21%	2.38%

Table 5. Envelope diagram key data.

tangential direction of the cutting edge, normal resistance in the normal direction, and the resistance moment acting on the cutting edge point[22].

The resistance, resistance moment, and forces at the hinge points of each component obtained through experimental calculations are imported into ADAMS in the form of spline curves. Simultaneously, angular drives are added to the hinge points A between the base and boom, B between the boom and arm, and the hinge points G between the arm and the bucket. The three joint angle change data are also added to the drive function in the same manner. The simulation time and step size are set, and the simulation is started.

Figures 8 and 9, and 10 show the (a) digging trajectory diagram, (b) cylinder stroke displacement curve diagram, (c) tooth tip load curve diagram, and (d) hinge point force comparison diagram for three different digging depths: surface digging, 1 M digging, and 2 M digging, respectively.

It can be seen from Figs. 8, 9 and 10b that each hydraulic cylinder exhibits distinct motion laws during the digging process. The boom mainly serves to lower and lift during the digging process. Here, the focus is on the digging process after the bucket comes into contact with the soil. As can be seen from the figure, the displacement change of the hydraulic cylinder of the boom is small, and the boom is in the locked state. The arm hydraulic cylinder and the bucket hydraulic cylinder are in a coordinated working state. In surface digging, it can be seen from Fig. 8c that the normal resistance no longer increases after 2 s, and the main digging function of the arm hydraulic cylinder. At the digging depths of 1 M and 2 M, it can be seen from Figs. 9c and 10c that both the digging resistance and the resistance moment vary significantly. Therefore, during the digging process, the coordinated displacement of the arm hydraulic cylinder and the bucket hydraulic cylinder is achieved, and the soil cutting is accomplished through their combined motion. From the simulation results, it can be seen that the displacement changes of the hydraulic cylinder are well matched, achieving efficient digging actions of the working device.

Figures 8, 9 and 10d show the comparison of the simulation values and experimental values of the forces acting on the three key hinge points of the working device. It can be seen from the figure that the force change at the hinge point A between the base and the boom is that the force change is relatively small in the first half of the digging, while in the second half, as the amount of soil in the bucket increases, the force value increases. The force values at the hinge point B between the boom and the arm and at the hinge point C between the arm and the bucket start to increase as soon as the bucket comes into contact with the soil. As the digging continues, the tangential resistance and normal resistance gradually increase. The resistance moment first decreases, then increases, and then increases in the opposite direction. Therefore, the force values at the hinge points continue to increase and eventually maintain a stable value under the thrust of the oil cylinder. Ultimately, as the tangential resistance gradually decreases from its peak, the forces acting on each hinge point also gradually decrease.

It can be seen from the Figs. 8 and 9, and 10d that the overall trend of the force simulation values is consistent with the experimental values. The errors at hinge point B and hinge point C are extremely small, while the error at hinge point A is slightly larger. This is because the force conditions at the hinge point between the base and the boom are the most complex. Besides the thrust from the boom hydraulic cylinder, there are also the inertial forces of the soil, the cumulative errors of the forces on the arm and the bucket, and the balance force of the

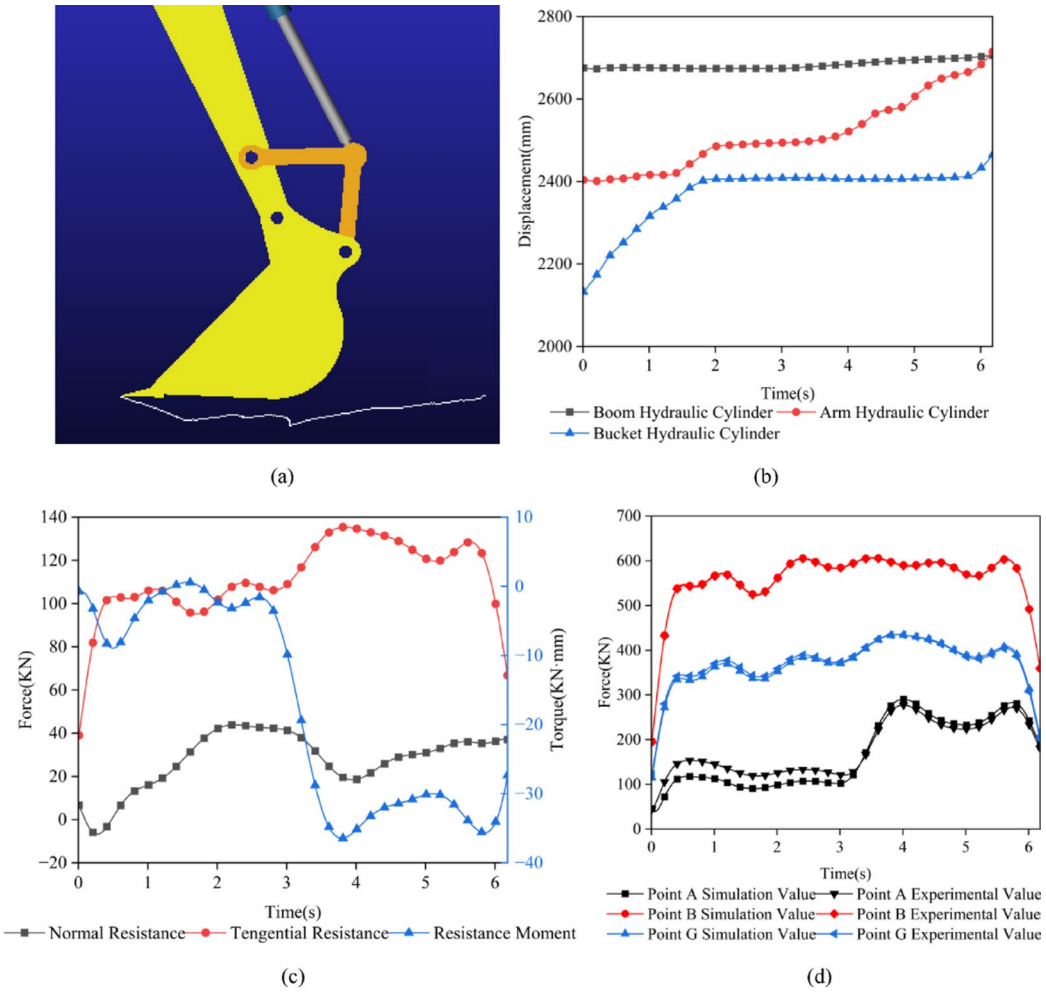

Fig. 8. Surface digging depth.

entire vehicle. The combined effect of these forces and the simplification of the simulation model make it difficult for the simulation model to fully capture its true force conditions.

To more accurately quantify the discrepancy between simulation and experimental values, the correlation coefficient (R) and root mean square error (RMSE) are introduced to rigorously and comprehensively validate model accuracy. R measures the linear correlation strength and direction between two variables ($-1 < R < 1$); the closer R is to 1, the higher the correlation between the variables. RMSE reflects the deviation between two variables; a smaller RMSE indicates less deviation. Table 6 lists the R for the force curves at each hinge point across three different digging depths. Figures 11, 12 and 13 display the RMSE histograms for the hinge force curves. Figures 11 and 12, and 13 present the RMSE plots for surface digging, 1 M digging, and 2 M digging, respectively. Each plot includes the three hinge points A, B, and G. Among the three digging depths, point A exhibits the highest RMSE value, indicating the greatest error at this point. This phenomenon aligns with point A having the lowest correlation coefficient. The maximum RMSE at point A is approximately 1.8 kN, at point B approximately 0.23 kN, and at point G approximately 0.55 kN. Compared to the force values at each point, this error is extremely small, with the maximum RMSE at each point accounting for less than 2% of the joint force value. A comprehensive analysis of the R and RMSE reveals that, despite the relative increase in RMSE values for the forces at each hinge point at a 2 M digging depth due to increased load uncertainty, the R remain above 0.97, indicating strong correlation and high model accuracy. This result demonstrates the model's excellent performance in capturing the dynamic trends of force changes at the hinge points. The increase in RMSE values with excavation depth further confirms that load uncertainty is a primary source of model error.

Electromechanical-hydraulic joint simulation and verification

This study systematically compares the dynamic response characteristics of the oil pressure of each hydraulic cylinder in the time domain based on the combined simulation of mechanics, electricity and hydraulics. The correlation coefficient and the difference between the oil pressure experimental value and the simulation value are used to objectively evaluate and verify the joint simulation model. In the combined simulation of mechanics, electricity and hydraulics, multiple sets of PID parameters were used for adjustment to obtain the simulated oil pressure values of the arm hydraulic cylinder and the bucket hydraulic cylinder, which were compared with

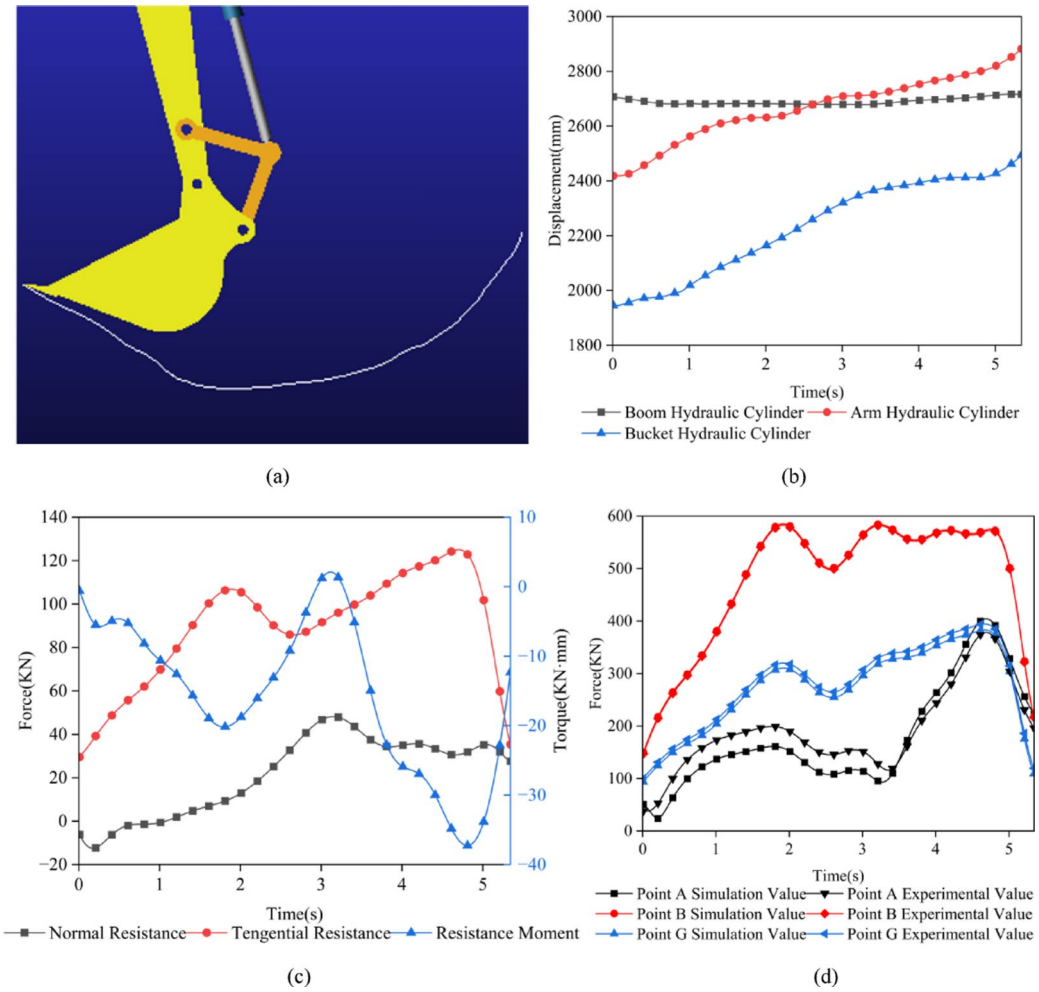

Fig. 9. 1 M digging depth.

the experimental values. This study focuses on verifying the joint simulation of electro-hydraulic systems and multibody dynamics. Despite the limitations of model simplification and some experimental parameters, by systematically comparing the dynamic response characteristics of different working conditions and different hydraulic cylinders, the research results fully confirm that the proposed joint simulation method can effectively capture the key features of the coupling effect between electro-hydraulic systems and multibody dynamics. This verified the reliability of the joint simulation model.

During the digging process, after the bucket comes into contact with the soil, the boom hydraulic cylinder is in a locked state and does not participate in the digging. The arm hydraulic cylinder and the bucket hydraulic cylinder work together to complete the compound digging. Therefore, this paper focuses on the collaborative working characteristics of the arm hydraulic cylinder and the bucket hydraulic cylinder. Figures 14, 15 and 16 shows the variation values of hydraulic cylinder oil pressure at different digging depths. The figure includes the simulation values, experimental values and the error values between the simulation and the experiment of the oil pressure.

Based on the changes in the load at the tip of the bucket tooth in Figs. 8, 9 and 10 (c), the dynamic characteristics of the oil pressure in each hydraulic cylinder at different digging depths are analyzed as follows. During surface digging, the resistance change is relatively stable. The resistance moment increases and stabilizes at a certain value after the bucket is filled with soil. Therefore, it can be seen from Fig. 14 that the oil pressure of the arm rod hydraulic cylinder and the bucket hydraulic cylinder at this digging depth first increases and then stabilizes. During the 1 M and 2 M digging, the changes in resistance and resistance moment are relatively large. As the amount of soil in the bucket increases, it can be seen from Figs. 15 and 16 that to overcome the resistance, the pressure of the hydraulic cylinder continuously increases to complete the digging. After the digging is completed, the boom performs a lifting action, reducing the digging resistance, and the oil pressure in the arm hydraulic cylinder and the bucket hydraulic cylinder gradually decreases. The changes in the oil pressure of the hydraulic cylinder adapt to the different load requirements during the digging process, ensuring the stable operation of the working device. As can be seen from Fig. 15, during the 2–3 s of 1 M digging, the pressure of the hydraulic cylinder first decreases and then increases, which is consistent with the tangential resistance change in Fig. 9c. This precisely indicates that the tangential resistance has the greatest influence during the digging

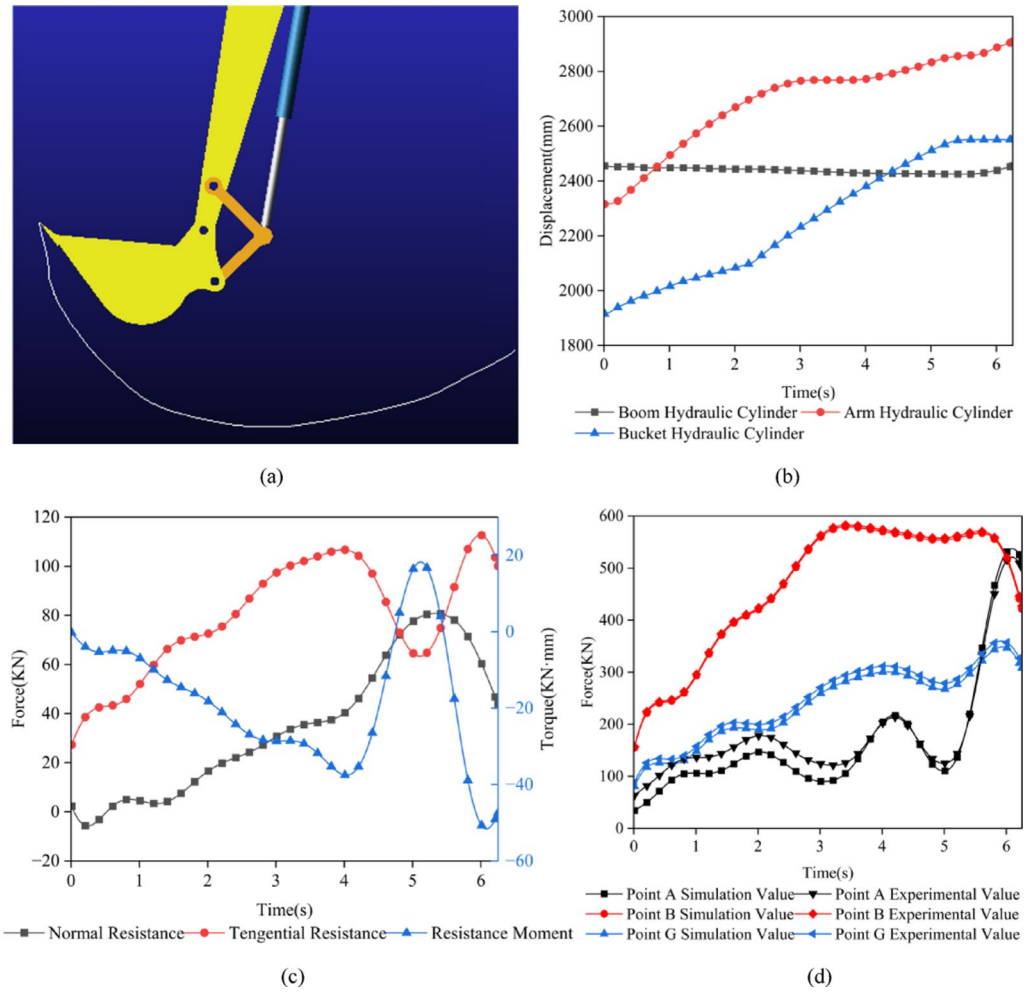

Fig. 10. 2 M digging depth.

Varying depths	Articulation point	Correlation coefficient
Surface digging	Base and boom articulation point	0.992
	Boom and arm articulation point	0.999
	Arm and bucket articulation point	0.995
1 M digging	Base and boom articulation point	0.979
	Boom and arm articulation point	0.999
	Arm and bucket articulation point	0.999
2 M digging	Base and boom articulation point	0.996
	Boom and arm articulation point	0.999
	Arm and bucket articulation point	0.999

Table 6. Comparison of simulation and experimental curves of hinge point force.

process. The same is true for the changes in cylinder pressure and tangential resistance in the second second of the 2 M digging.

As shown in Figs. 14, 15 and 16, the simulated hydraulic pressure values of the hydraulic cylinder generally align with the experimental values, but there are some discrepancies. This is because the hydraulic system and mechanical structure of the working device have been simplified to some extent, neglecting factors such as the elastic deformation of hydraulic pipes, the compressibility of hydraulic fluid, and the elastic deformation of the actual structure. These factors can influence hydraulic pressure in real-world applications. Additionally, in the experiments, the digging load inherently has some uncertainty due to the objective conditions of the experimental site, and these uncertainties are difficult to replicate in the simulation, leading to discrepancies between the experimental and simulated results. However, after multiple simulations and adjustments to the

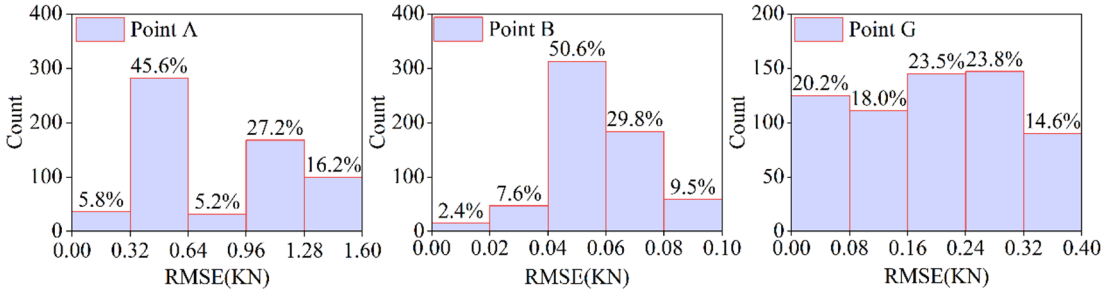

Fig. 11. Surface digging depth.

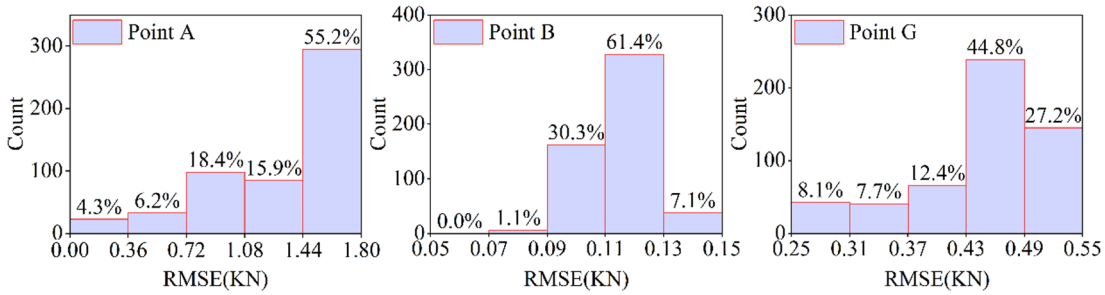

Fig. 12. 1 M digging depth.

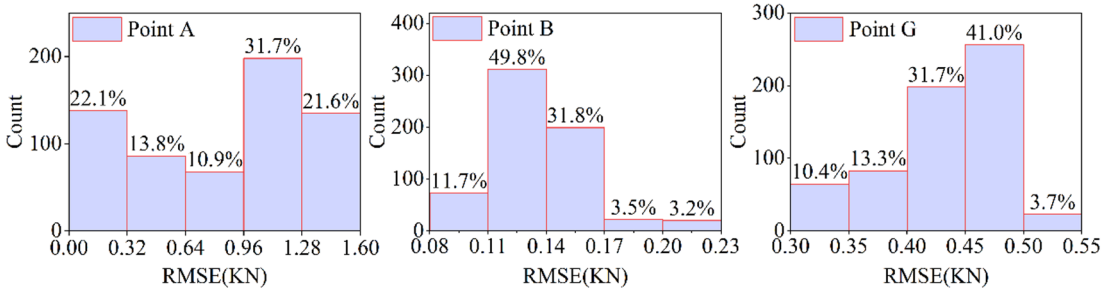

Fig. 13. 2 M digging depth.

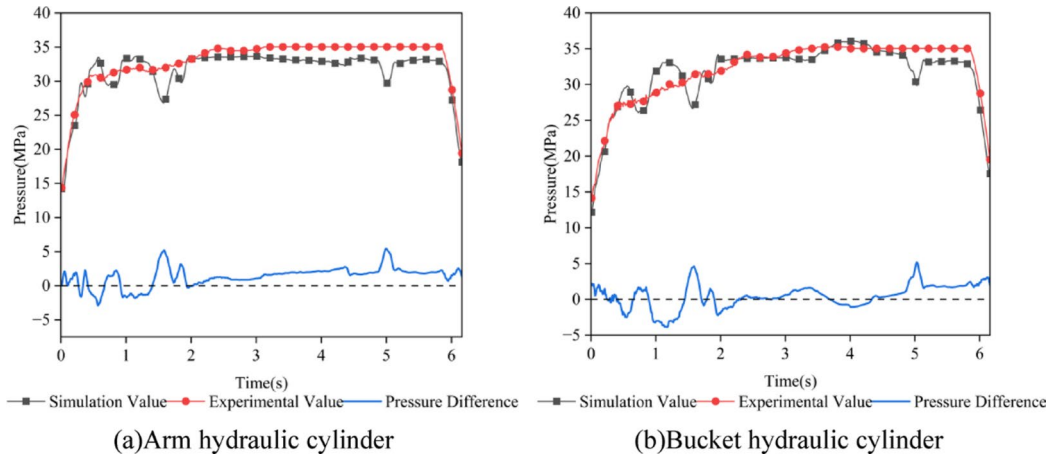

Fig. 14. Surface digging depth.

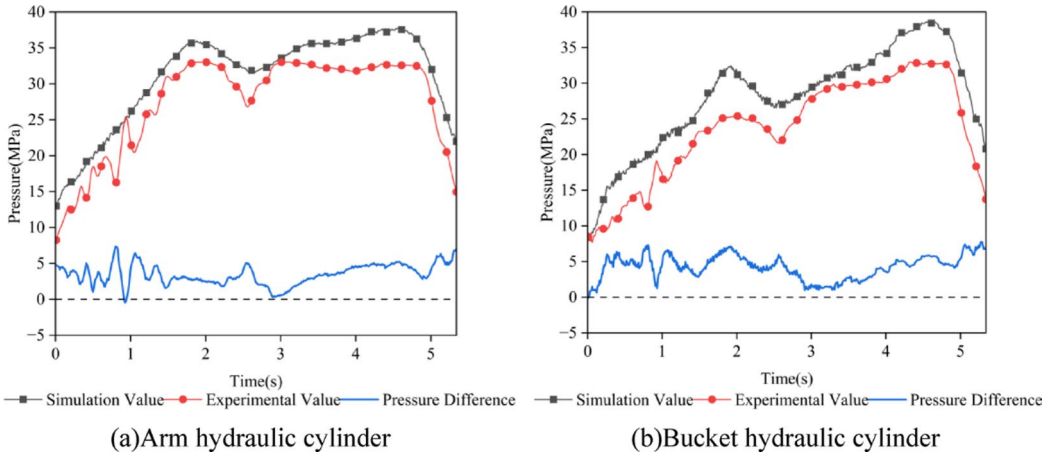

Fig. 15. 1 M digging depth.

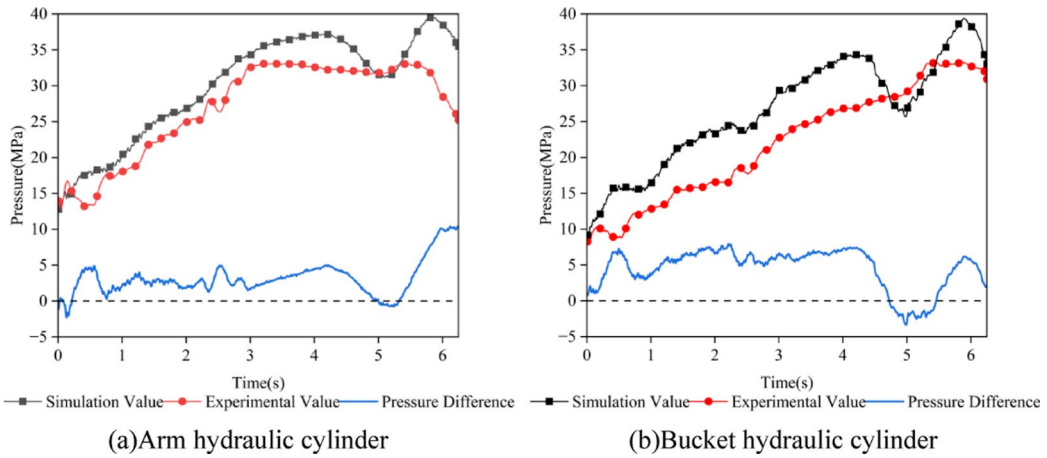

Fig. 16. 2 M digging depth.

parameters, the experimental and simulated values of the hydraulic pressure in the arm cylinder and bucket cylinder at various digging depths generally follow the same trend, with the error gradually decreasing. Figures 14, 15 and 16 show the difference curves between simulation values and experimental values. During surface digging, the difference is generally around 2 MPa, with the difference accounting for approximately 5% of the simulation value. Two fluctuations reached 5 MPa, with the maximum error accounting for about 15% of the simulation value. During the first 2 s of 1 M and 2 M digging, as the digging depth increases, resistance gradually increases, leading to larger fluctuations in the experimental hydraulic cylinder oil pressure values, which in turn cause larger fluctuations in the different values. This is unavoidable in actual digging experiments; After 2 s, the digging enters a stable phase, with the difference fluctuating around 5 MPa, and the ratio of the difference to the simulated value remains relatively stable at 15%. However, during the final digging phase, due to the rapid decrease in digging resistance, particularly the rapid decrease in tangential resistance, the hydraulic cylinder oil pressure experiences significant fluctuations, leading to a larger difference between the simulated and experimental values. This further highlights the critical role that changes in tangential resistance during the digging process play in affecting other components.

To more accurately illustrate the precision of cylinder pressure in the joint simulation, Table 7 below lists the R values for the oil pressure curves of each hydraulic cylinder at three different digging depths. Figures 17, 18 and 19 display the RMSE histograms of the oil pressure curves. As shown in Figs. 17, 18 and 19, with increasing digging depth, the maximum RMSE value of the arm cylinder pressure rises from 0.25 MPa to 0.45 MPa, with its proportion of the total dataset gradually increasing. Similarly, the maximum RMSE value for the bucket hydraulic cylinder pressure increased from 0.25 MPa to 0.35 MPa, also with its proportion of the total dataset gradually increasing, yet its R remained above 0.9. Across the three digging depths, the maximum RMSE values for each hydraulic cylinder pressure accounted for approximately 5% or less of the working pressure. This result indicates that the model excellently captures the dynamic variation trends of hydraulic cylinder pressures, while its absolute error level remains within an engineering-acceptable reasonable range.

Different depths	Hydraulic cylinder	Correlation coefficient
Surface digging	Arm hydraulic cylinder	0.908
	Bucket hydraulic cylinder	0.931
1 M digging	Arm hydraulic cylinder	0.975
	Bucket hydraulic cylinder	0.970
2 M digging	Arm hydraulic cylinder	0.907
	Bucket hydraulic cylinder	0.931

Table 7. Comparison between simulation and experimental curves of oil pressure values.

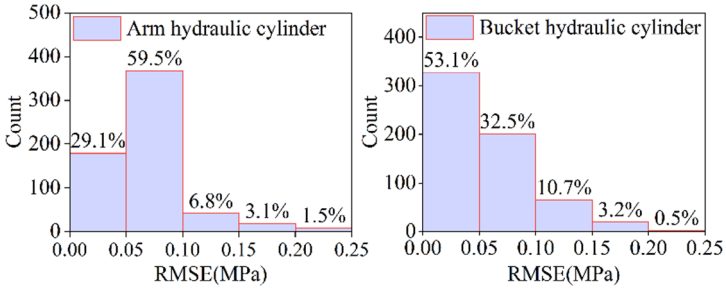

Fig. 17. Surface digging depth.

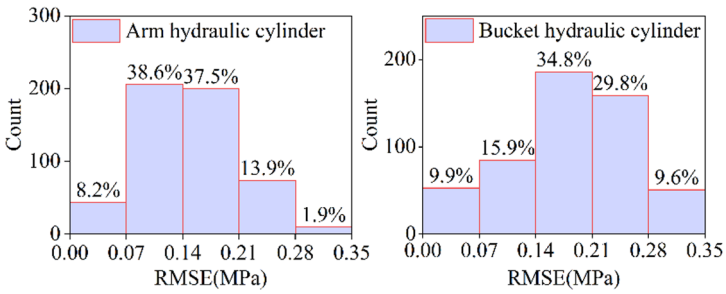

Fig. 18. 1 M digging depth.

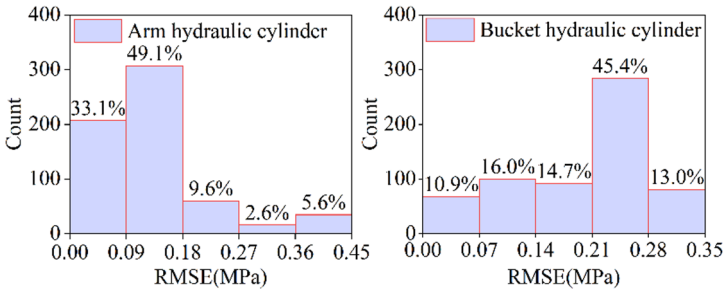

Fig. 19. 2 M digging depth.

In summary, the displacement of the hydraulic cylinder and the load on the bucket tooth of the hydraulic excavator's working device show certain changes, while the changes in hydraulic cylinder oil pressure adapt to the load requirements and are consistent with the actual situation. In subsequent research, it is still necessary to consider multiple factors more comprehensively and accurately to improve the accuracy of the joint simulation model, thereby enhancing the accuracy and reliability of the simulation model and providing more effective guidance for the design and optimization of the hydraulic excavator's working device.

Conclusions and future work

This study developed a high-fidelity, data-driven mechatronic-hydraulic co-simulation model based on a 20-ton backhoe hydraulic excavator. The model underwent systematic validation using field-measured data. Results demonstrate that this co-simulation model effectively predicts working device performance, providing theoretical foundations and technical support for structural optimization and intelligent control development in hydraulic excavators. The research holds significant scientific value and engineering contributions in method integration and validation rigor, specifically manifested in:

(1) A simulation validation framework driven by actual measurement data. Unlike most simulation studies relying on theoretical loads or simplified assumptions, this paper utilizes field-collected hydraulic cylinder pressure and joint angle data. Through a resistance model developed by the author's team, digging resistance is calculated and input as load into the integrated simulation model. This method of validation using actual measurement data ensures the authenticity of the model's load conditions, significantly enhancing its predictive capability and credibility under real operating conditions.
(2) Implementation of Multisoftware Collaboration and Bidirectional Coupling Mechanism. This paper utilizes ADAMS and AMESim to construct a joint simulation model featuring bidirectional coupling between dynamics and hydraulics. Model integration is achieved through the FMI standard. This coupling mechanism precisely captures the dynamic interactions between systems, revealing the underlying mechanism of how hydraulic cylinder pressure dynamically responds and drives the working device to perform compound actions under varying digging depths and loads. It provides a reusable technical approach for integrated modeling of complex electromechanical-hydraulic systems.
(3) Multilevel, multiphysical quantity systematic validation. This study not only completed hierarchical validation from kinematics to dynamics and joint simulation but also conducted systematic comparisons across three typical digging depths. It comprehensively assessed the simulation accuracy of key parameters such as hinge forces and hydraulic cylinder pressures: Envelope diagram kinematic indicators showed minimal error ($<5\%$); critical hinge forces ($R>0.979$, RMSE <1.8); hydraulic cylinder pressure ($R>0.907$, RMSE <0.45). This multilevel, multiphysical verification significantly enhances the model's credibility, positioning it as a core model for high-performance digital twin systems. It lays a solid foundation for subsequent research in condition prediction and intelligent control strategy optimization.

Although this study validated the effectiveness of the joint simulation model under specific operating conditions through measured data, certain limitations remain. The current resistance model treats loads as concentrated forces and does not account for soil mechanical properties (such as cohesion in different soil types), complex digging interfaces (such as dynamic geometric changes during slope excavation), or the dynamics of bucket-soil interactions. These factors are significant sources of uncertainty and dynamic complexity in actual loads, contributing to simulation deviations. A key future research direction involves coupling the validated electromechanical-hydraulic model from this study with a high-fidelity discrete element model. This integration will simulate bucket-soil interactions at the micro-mechanical level, dynamically generating excavation resistance. Such an approach will expand the model's predictive capability and universality, providing valuable insights for developing intelligent excavation strategies and designing high-performance excavators.

Data availability

The dataset generated during the current study period can be obtained from the corresponding author upon reasonable request.

Received: 3 September 2025; Accepted: 17 November 2025
Published online: 26 November 2025

References

1. Chen, F. et al. Matching performances for Hydraulie system based on multi-disciplinary collaborative simulation. *Opencast Min. Technol.* **31**(5), 573–577. (2014). https://doi.org/10.3969/j.issn.1001-4551.2014.05.007
2. Zhang, G. et al. Dynamic analysis and simulation of excavator working device based on virtual prototype technology. *J. Cent. South. Univ. (Sci. Technol.)*. **45**(6), 1827–1833 (2014).
3. Jiang, X. et al. Dynamics simulation analysis of hydraulic excavator's working equipment based on ADAMS. *Mod. Manuf. Eng.*(11), 74–77. https://doi.org/10.16731/j.cnki.1671-3133.2014.11.023 (2014).
4. Zhu, M. et al. Design and research of automatic leveling system for three degrees of freedom hydraulic boom.*Mach. Tool. Hydraulics*. **52**(9), 94–99. (2024). https://doi.org/10.3969/j.issn.1001-3881.2024.09.014
5. Bao, J., Li, J. & Wang, H. Hydraulic excavator load sensing hydraulic control system AMESim simulation analysis. *Constr. Mach. Equip.* **53**(7), 56–63 (2022).
6. Zhang, T. et al. Digital twin-driven excavation trajectory planning of unmanned excavator based on multidisciplinary co-simulation. *Autom. Constr.* **178**, 106404. https://doi.org/10.1016/j.autcon.2025.106404 (2025).
7. Bender, F. A., Mitschke, M., Bräunl, T. & Sawodny, O. Predictive operator modeling for virtual prototyping of hydraulic excavators. *Autom. Constr.* **84**(1), 133–145. https://doi.org/10.1016/j.autcon.2017.08.008 (2017).
8. Song, X. et al. Multidisciplinary co-design optimization of the structure and control systems for large cable shovel considering cross-disciplinary interaction. *Proc. Inst. Mech. Eng., Part C: J. Mech. Eng. Sci.* **234**(22), 4353–4365. https://doi.org/10.1177/0954406220924464 (2020).
9. Park, C. G. et al. A coupled hydraulic and mechanical system simulation for hydraulic excavators. *Proc. Inst. Mech. Eng., Part C: J. Mech. Eng. Sci.* **234**(4), 527–549. https://doi.org/10.1177/0959651819861612 (2020).
10. Jaiswal, S. et al. State estimator based on an indirect Kalman filter for a hydraulically actuated multibody system. *Multibody Sys. Dyn.* **54**(4), 373–398. https://doi.org/10.1007/s11044-022-09814-3 (2022).
11. Jaiswal, S. et al. Comparing double-step and penalty-based semirecursive formulations for hydraulically actuated multibody systems in a monolithic approach. *Multibody Sys.Dyn.* **52**(2), 169–191. https://doi.org/10.1007/s11044-020-09776-4 (2021).

12. Rahikainen, J., Mikkola, A., Sopanen, J. & Gerstmayr, J. Combined semi-recursive formulation and lumped fluid method formonolithic simulation of multibody and hydraulic dynamics. *Multibody Sys.Dyn.* **44**(3), 293–311. https://doi.org/10.1007/s11044-018-9631-x (2018).
13. Zhou, Y. et al. Combined simulation of excavator digging motion track control based on Adams and Amesim. *Mach. TOOL. HYDRAULICS*. **49**(4), 146–150. https://doi.org/10.3969/j.issn.1001-3881.2021.04.029 (2021).
14. Zhang, W., Yang, G., Zhou, W. & Peng, X. Study on motion planning and control of intelligent excavator in linear excavation. *J. Hunan Univ. (Natural Sciences)*. **50**(6), 70–79. https://doi.org/10.16339/j.cnki.hdxbzkb.2023171 (2023).
15. Wang, G. et al. Research on collaborative locking strategy for distributed locking system of space manipulator. *Proc. Inst. Mech. Eng., Part C: J. Mech. Eng. Sci.* **238**(23), 11068–11080. https://doi.org/10.1177/09544062241277315 (2024).
16. Gan, J. et al. Co-simulation of multibody dynamics and discrete element method for hydraulic excavators. *Powder Technol.* **414**, 118001. https://doi.org/10.1016/j.powtec.2022.118001 (2023).
17. Liu, B. et al. Investigation of performance of hydraulic excavators by co-simulation of multibody dynamics and discrete element method. *Powder Technol.* **414**, 118088. https://doi.org/10.1016/j.powtec.2022.118088 (2023).
18. Jin, L., Li, Y. & Zeng, H. Simulation analysis and modeling of a large hydraulic excavator based on ADAMS, *Mod. Manuf. Eng.* **11**, 100–104, 109. https://doi.org/10.16731/j.cnki.1671-3133.2017.11.018 (2017).
19. Liu, C., Sun, J. & Shi, D. Dynamic modeling and analysis for hydraulic excavator working device. *Mach. Tool. Hydraulics*. **49**(7), 156–159. https://doi.org/10.3969/j.issn.1001-3881.2021.07.030 (2021).
20. Ren, Z. et al. Active-Side calculation method for a backhoe hydraulic excavator with incomplete digging resistance in a normal state. *Math. Probl. Eng.*(1), 1–13. https://doi.org/10.1155/2019/9846305 (2019).
21. Long, Z. et al. Review of research state of trajectory planning for industrial robots. *Mech. Sci. Technol. Aerosp. Eng.* **40**(6), 853–862. https://doi.org/10.13433/j.cnki.1003-8728.20200132 (2021).
22. Chen, J., Ren, Z., Lv, L. & Yong, B. Modeling of the compound digging force of hydraulic excavator based on resistance characteristics. *J. Northeastern Univ. (Natural Science)*. **36**(7), 1015–1019. https://doi.org/10.3969/j.issn.1005-3026.2015.07.022 (2015).

Author contributions

All the authors contributed to this research. Mei Xin was primarily responsible for the conception and writing of the paper. Zhigui Ren was primarily responsible for obtaining funding for the paper and guiding revisions. Yiding Yu and Yudong Tian were primarily responsible for assisting with the simulation. Heng Zhang, Kaitao Ren, and Yijian Zhang were primarily responsible for proofreading the paper.

Funding

This research was supported by the Key Research Program Project of Shaanxi Provincial Department of Science and Technology (No. 2024NC-YBXM-203) and the Shaanxi Provincial Department of Education Service Local Special Industrialization Cultivation Project (No. 24JC024).

Declarations

Competing interests

The authors declare no competing interests.

Additional information

Correspondence and requests for materials should be addressed to Z.R.